Luminescence properties of Ce^{3+}-doped $LiGdP_4O_{12}$ upon vacuum-ultraviolet and x-ray excitation

2009 J. Phys.: Condens. Matter 21 445901

(http://iopscience.iop.org/0953-8984/21/44/445901)

J. Phys.: Condens. Matter **21** (2009) 445901 (8pp) doi:10.1088/0953-8984/21/44/445901

Luminescence properties of Ce^{3+}-doped $LiGdP_4O_{12}$ upon vacuum-ultraviolet and x-ray excitation

T Shalapska[1], G Stryganyuk[1,2], P Demchenko[1], A Voloshinovskii[1] and P Dorenbos[3]

[1] Physics Department, Ivan Franko National University of Lviv, 8 Kyryla i Mefodiya Street, 79005 Lviv, Ukraine
[2] Institute for Scintillation Materials, NAS of Ukraine, 60 Lenina Avenue, 6100 Kharkiv, Ukraine
[3] Delft University of Technology, 15 Mekelweg, 2629 JB Delft, The Netherlands

E-mail: t_shalapska@ukr.net

Received 23 July 2009, in final form 15 September 2009
Published 9 October 2009
Online at stacks.iop.org/JPhysCM/21/445901

Abstract
Luminescent-kinetic studies for $LiY_{0.9}Ce_{0.1}P_4O_{12}$, $LiGd_{0.9}Ce_{0.1}P_4O_{12}$ and $NaGd_{0.9}Ce_{0.1}P_4O_{12}$ phosphates which were prepared by the melt solution technique have been performed using synchrotron radiation excitation within 3–12.4 eV energy range and x-ray radiation at $T = 10$–300 K. The Ce $\rightarrow$ Gd transfer at 10 K and bidirectional Ce $\leftrightarrow$ Gd mechanisms of energy transfer at 300 K have been revealed based on the analysis of the excitation spectra and decay kinetic measurements of Ce^{3+} luminescence. The participation of the Gd sublattice in the energy migration process to the Ce^{3+} centers causes the appearance of a slow component in the decay kinetics of the x-ray-excited luminescence pulse. The luminescence efficiency of $LiY_{0.9}Ce_{0.1}P_4O_{12}$, $LiGd_{0.9}Ce_{0.1}P_4O_{12}$ and $NaGd_{0.9}Ce_{0.1}P_4O_{12}$ upon x-ray excitation at room temperature is discussed.

1. Introduction

Stoichiometric oxide compounds based on lanthanides are considered as promising luminescent materials for different applications. For such types of compounds a relatively long distance between lanthanide ions is typical. This fact facilitates decreased concentration quenching and helps in achieving high emission intensities. The chemical stability of oxide compounds and their relative simplicity of synthesis in powder form attracts attention to these materials.

A special interest in rare earth polyphosphates is caused by the potential of their luminescence properties for lasing and lighting applications. $LiNdP_4O_{12}$ is known as an active element of microlasers. Recently, $NaGd(PO_3)_4$:Tb^{3+} was reported to be a new promising green phosphor for plasma display panel applications [1]. Some polyphosphates could be useful as efficient scintillators or for x-ray detection as well. In particular, Zhong *et al* found that Ce^{3+} luminescence of $NaGd(PO_3)_4$:10.0 at.% Ce^{3+} powder samples offers a high light yield (21 000 photon MeV^{-1}) and short decay time constant of about 12.4 ns [2]. Luminescence properties of $AGdP_4O_{12}$ (A = Li, Na, K, Cs) with 1.0 at.% Ce^{3+} were studied in detail at 300 K [3].

The Gd-containing phosphors are also interesting due to possible achievement of high light yields if doped with Ce^{3+} ions. This is due to an effective energy transfer from the Gd sublattice to the emission center, when the Ce^{3+} ions' absorption band coincides with the energy of the $^6P_{7/2} \rightarrow {}^8S_{7/2}$ radiative transition ($\lambda = 312$ nm) in Gd^{3+}. The main drawback of Gd-based compounds is a probable slow decay component in the scintillation pulse caused by the slow migration of excitation energy through the Gd sublattice. In some cases substantial shortening of the duration of this slow component [4] or even complete absence, as in the case of $Gd_2(SiO_4)O$:Ce^{3+} [5], has been achieved.

Here we report on the investigation of the luminescent characteristics of $LiGd_{0.9}Ce_{0.1}P_4O_{12}$, $NaGd_{0.9}Ce_{0.1}P_4O_{12}$ and $LiY_{0.9}Ce_{0.1}P_4O_{12}$ powder samples upon excitation with high energy quanta of synchrotron radiation in the VUV–UV range and x-ray quanta. The work was performed in order to

Table 1. Crystallographic data for polyphosphates.

No.	Formula	Space group	Cell parameters				Reference
			a (Å)	b (Å)	c (Å)	β (deg)	
1	$LiGd_{0.9}Ce_{0.1}P_4O_{12}$	$C2/c$	16.323(3)	7.031(5)	9.575(2)	126.021(1)	Our work
2	$LiGd(PO_3)_4$	$C2/c$	16.386(2)	7.509(3)	9.677(2)	126.121(1)	[14]
3	$LiY(PO_3)_4$	$C2/c$	16.201(4)	7.013(2)	9.573(2)	125.589(9)	[13]
4	$NaGd(PO_3)_4$	$P2_1/n$	9.767(3)	13.01(1)	7.160(2)	90.564(5)	[11]

elucidate the mechanism of the excitation energy migration and the transfer processes involving the Gd sublattice, electron–hole pairs and excitons in the scintillation material of $AGdP_4O_{12}$ (A = Li, Na) type doped with cerium.

Taking into account that a maxima light yield for $NaGd(PO_3)_4:Ce^{3+}$ powder sample has been obtained for 10 at.% Ce^{3+} [2], special attention is focused towards $AGdP_4O_{12}$ (A = Li, Na) with 10 at.% of Ce^{3+} under excitation using synchrotron and x-ray radiation.

2. Experimental procedures

$LiGd_{0.9}Ce_{0.1}P_4O_{12}$, $NaGd_{0.9}Ce_{0.1}P_4O_{12}$ and $LiY_{0.9}Ce_{0.1}P_4O_{12}$ powder samples were prepared using the melt solution technique. For the synthesis of these polyphosphates, Li_2CO_3, Na_2CO_3, $NH_4H_2PO_4$, Y_2O_3, Gd_2O_3 and CeO_2 were used as starting materials. These reagents were mixed and fired in quartz crucibles at 700 °C for 2 h.

X-ray powder diffraction data were collected on an automatic diffractometer STOE STADI P with a linear position-sensitive detector (PSD) with the following characteristics: transmission mode, $2\theta/\omega$ scan; Cu Kα_1 radiation, curved germanium [1 1 1] monochromator; 2θ range $6.000° \leqslant 2\theta \leqslant 124.545°$ 2θ with step 0.015° 2θ; PSD step 0.480° 2θ, scan time 300 s/step.

Preliminary data processing, x-ray profile and phase analyses were performed using the STOE WinXPOW version 2.21 program package [6]. The crystal structure was refined from powder diffraction data with the program FullProf.2k (version 4.00) [7] from the WinPLOTR software [8], using a pseudo-Voigt profile function. The crystallographic data were standardized with the program Structure Tidy [9].

The study of the microstructure of the $LiGd_{0.9}Ce_{0.1}P_4O_{12}$ and $NaGd_{0.9}Ce_{0.1}P_4O_{12}$ crystals were carried out using a JEOL JSM-T220A scanning electron microscope with x-ray analyzer (dispersion Si (Li) detector). Elemental composition of the samples was studied using this analyzer directly in the microscope chamber. Micrographs were obtained by means of a secondary-electron registration mode.

Measurements of luminescence excitation and emission spectra as well as decay kinetics were performed upon excitation by synchrotron radiation from the DORIS storage ring (DESY, Hamburg) using the facility of the SUPERLUMI station at HASYLAB [10]. The measurements were carried out at 10 and 300 K. Emission spectra were measured within 250–600 nm range using an ARC 'Spectra Pro 308' 30 cm monochromator-spectrograph in a Czerny-Turner mounting equipped with a CCD detector from Princeton Instruments. Time-resolved luminescence excitation spectra were scanned with a resolution of 3.2 Å within 340–100 nm by the primary 2 m monochromator in a 15° McPherson mounting using a HAMAMATSU R6358P PMT at the secondary ARC monochromator. Integral mode spectra correspond to the integral number of photons detected by a photomultiplier. Fast component spectra were registered by photon counting just after the excitation pulse within a 2–20 ns time gate. For slow component spectra the gate duration was set at 150–200 ns. Luminescence excitation spectra have been corrected for the incident photon flux by means of Na-salycilate. Luminescence decay kinetic curves were accumulated within a 200 ns range using a single-photon counting technique.

The x-ray-excited emission spectra and decay kinetics studies were performed employing excitation by a laboratory x-ray source (anode voltage 40 kV, current intensity 0.2 mA) with pulse duration of 2 ns and repetition frequency of 100 kHz.

3. Sample characterizations

X-ray diffraction patterns indicate that the $LiY_{0.9}Ce_{0.1}P_4O_{12}$, $LiGd_{0.9}Ce_{0.1}P_4O_{12}$ and $NaGd_{0.9}Ce_{0.1}P_4O_{12}$ crystals were crystallized in monoclinic symmetry with space group $C2/c$ for $LiY_{0.9}Ce_{0.1}P_4O_{12}$ and $LiGd_{0.9}Ce_{0.1}P_4O_{12}$ and $P2_1/n$ for $NaGd_{0.9}Ce_{0.1}P_4O_{12}$. More detailed x-ray diffraction analysis has been performed on $LiGd_{0.9}Ce_{0.1}P_4O_{12}$. The XRD pattern of this polycrystalline sample shows the presence of $LiGd_{0.9}Ce_{0.1}P_4O_{12}$ single phase, i.e. a solid solution of cerium in $LiGdP_4O_{12}$. Comparison of experimental and calculated powder patterns is presented in figure 1.

It should be noticed that a strongly preferred orientation effect for phase grains was observed along the [100] direction, despite the fact that x-ray transmission geometry was used. The crystal structure of the $LiGd_{0.9}Ce_{0.1}P_4O_{12}$ phase is isotypic with $LiNd(PO_3)_4$ [12], and our results agree with data for the parent compound $LiGd(PO_3)_4$ [14]. Crystallographic data for $LiYP_4O_{12}$, $NaGd(PO_3)_4$ and $LiGd_{0.9}Ce_{0.1}P_4O_{12}$ are given in table 1.

The microstructure of the $LiGd_{0.9}Ce_{0.1}P_4O_{12}$ and $NaGd_{0.9}Ce_{0.1}P_4O_{12}$ samples is shown in figures 2(a) and (b). $LiGd_{0.9}Ce_{0.1}P_4O_{12}$ microcrystals of 5 μm and $NaGd_{0.9}Ce_{0.1}P_4O_{12}$ of 100 μm size are observed in the micrographs. Different sizes of microcrystals can influence the spectral properties and luminescence efficiency of these polyphosphates. The structure of $LiGd_{0.9}Ce_{0.1}P_4O_{12}$ and $NaGd_{0.9}Ce_{0.1}P_4O_{12}$ was further verified by the spectroscopic data and it is in agreement with literature data [11, 14].

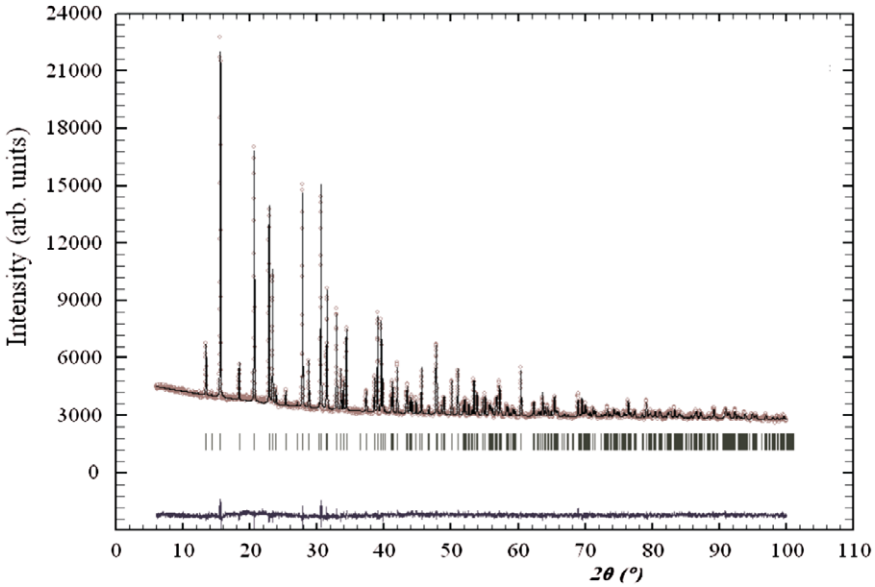

Figure 1. Observed and calculated x-ray powder profiles for sample $LiGd_{0.9}Ce_{0.1}P_4O_{12}$ (Cu Kα_1 radiation). Experimental data (circles) and calculated profile (solid line through the circles) are presented together with the calculated Bragg positions (vertical ticks) and difference curve (solid line).

(This figure is in colour only in the electronic version)

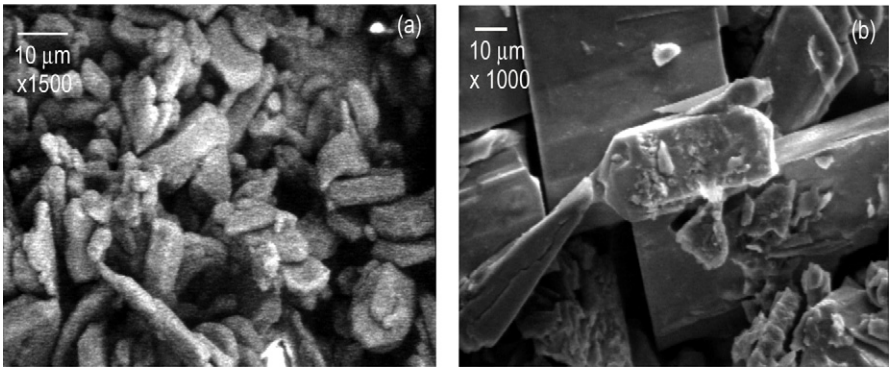

Figure 2. Microphotos of $LiGd_{0.9}Ce_{0.1}P_4O_{12}$ (a) and $NaGd_{0.9}Ce_{0.1}P_4O_{12}$ (b) obtained in the secondary-electron mode at different magnification.

4. VUV–UV luminescence spectroscopy results

4.1. Low temperature studies ($T = 10$ K)

The excitation and time resolved luminescence spectra of $LiGd_{0.9}Ce_{0.1}P_4O_{12}$ and $LiY_{0.9}Ce_{0.1}P_4O_{12}$ compounds are displayed in figure 3. The luminescence spectrum of $LiGd_{0.9}Ce_{0.1}P_4O_{12}$ shows UV emission bands peaked at 310 and 330 nm that are typical for the 5d–4f emission of Ce^{3+} ions, figure 3(a), curve 1. The energy separation between the two maxima is about 0.24 eV which is in good agreement with the usual spin–orbit splitting value of the Ce^{3+} ion 4f ground state. Thus, the observed luminescence bands can be attributed to the 5d–$^2F_{5/2}$ and 5d–$^2F_{7/2}$ transitions of Ce^{3+}.

The excitation spectrum of the 330 nm luminescence band reveals the presence of a structure typical for Ce^{3+} ion 5d energy levels in a low-symmetry crystal field of a dodecahedral coordination around Ce^{3+}, figure 3(a), curve 2. Compounds like YPO_4, $LiYF_4$ and Li_2CaSiO_4 show similar coordination around Ce^{3+} and also the 4f–5d excitation spectrum appears very similar, i.e. a low-lying excitation band is attributed to the x^2–y^2 5d orbital separated by almost 1 eV from the next 5d band attributed to the z^2 5d orbital. Both orbitals stem from the splitting of the cubic e_g level. The bands at 294 and 241 nm are attributed to these two orbitals. The next higher bands at 229 and 219 nm have zx and yz character, and the highest band at 187 nm is assigned to the xy 5d orbital. Those three bands all stem from the cubic t_{2g} orbital. Motivation of these assignments can be found in [15]. The total crystal field splitting, i.e. energy difference between highest and lowest energy 5d band, and the average energy of the five 5d bands agrees with expectation.

The decay curve of the 330 nm luminescence band reveals a single exponentially decaying curve with decay constant of $\tau = 9.5$ ns (figure 4, curve 2). Being relatively short, it is a non-typical value for decay time constant for cerium emission.

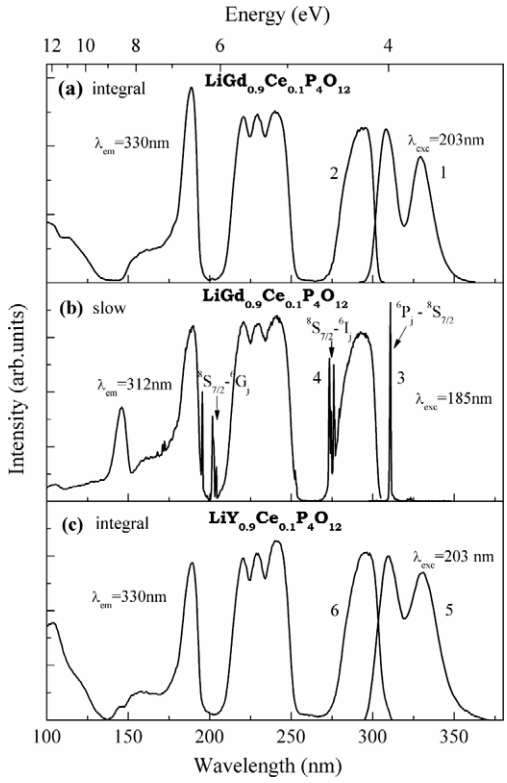

Figure 3. Excitation (2, 4, 6) and emission spectra (1, 3, 5) of $LiGd_{0.9}Ce_{0.1}P_4O_{12}$ and $LiY_{0.9}Ce_{0.1}P_4O_{12}$ at 10 K; (a) integral, (b) slow and (c) integral mode of registration.

Such a short decay time is attributed to energy transfer from Ce^{3+} ions to Gd^{3+} ions, possibly because the Ce^{3+} emission overlaps the $^8S_{7/2} \rightarrow {}^6P_{7/2}$ transition in Gd^{3+} ions.

The valley in the excitation spectrum in the region of $\lambda = 140$ nm coincides with the edge of the band-to-band transitions which was determined from the onset of the excitation spectrum of self-trapped exciton emission in $LiGdP_4O_{12}$ [16]. In the region of band-to-band excitations ($\lambda \leqslant 140$ nm) the decay kinetics of Ce^{3+} ions is also exponential with the constant of $\tau = 9.5$ ns coinciding with the decay time constant for the emission of Ce^{3+} ions upon excitation in the range of 4f–5d transitions. The absence of a long decay time component at band-to-band excitations can be caused by the process when, at high cerium concentrations, the electron–hole pairs recombine immediately with Ce^{3+} ions without trapping.

Similar Ce^{3+} ion spectral-luminescence characteristics are revealed in the luminescence of $LiY_{0.9}Ce_{0.1}P_4O_{12}$ (see figure 3(c), curves 5 and 6). The position of excitation and emission bands for $LiY_{0.9}Ce_{0.1}P_4O_{12}$ is almost identical to that for $LiGd_{0.9}Ce_{0.1}P_4O_{12}$. Such similarity confirms our finding from XRD data on the isomorphism of these two crystalline structures. It also points out that these polyphosphates crystallize in a monoclinic system with $C2/c$ space group with almost similar lattice parameters. In the decay kinetics of the 330 nm Ce^{3+} ion luminescence the fast component is present in the entire range of the excitation spectrum. The decay time constants for $LiY_{0.9}Ce_{0.1}P_4O_{12}$ ($\tau = 18.0$ ns) and

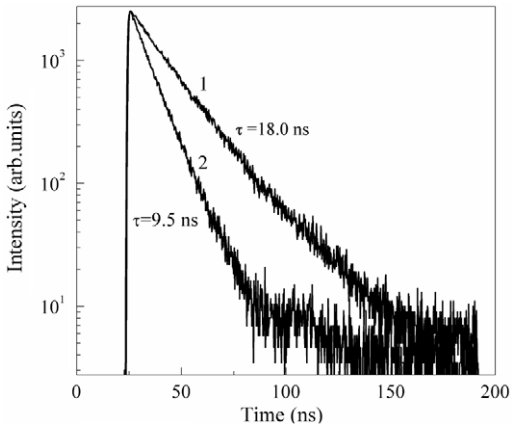

Figure 4. Luminescence decay curves of Ce^{3+} emission (330 nm) for $LiGd_{0.9}Ce_{0.1}P_4O_{12}$ (curve 2) and $LiY_{0.9}Ce_{0.1}P_4O_{12}$ (curve 1) under UV excitation (290 nm) at 10 K.

$LiGd_{0.9}Ce_{0.1}P_4O_{12}$ ($\tau = 9.5$ ns) are different as shown in figure 4. The decay time constant of 18 ns is regarded as the genuine lifetime of the Ce^{3+} 5d state. As mentioned, the decrease of the decay time to 9.5 ns is attributed to Ce → Gd energy transfer.

Energy back transfer from Gd^{3+} to Ce^{3+} was not revealed, and also not expected since the Gd^{3+} emission band at 312 nm ($^6P_{7/2} \rightarrow {}^8S_{7/2}$ transition) does not overlap the lowest energy excitation band of Ce^{3+}. The absence of such energy transfer is concluded from figure 3(b) (curves 4 and 3). The energy level structure of the Gd^{3+} ion is revealed in the excitation spectra of the Gd^{3+} $^6P_{7/2} \rightarrow {}^8S_{7/2}$ luminescence transition recorded in the slow time window with 150–200 ns time gate. Around 205 and 273 nm the typical sharp excitation lines corresponding to the $^8S_{7/2} \rightarrow {}^6G_j$ and $^8S_{7/2} \rightarrow {}^6I_j$ transitions are clearly seen.

The broad excitation band with maximum at 145 nm in figure 3(b), curve 4, is attributed to excitation of the phosphate groups with subsequent energy transfer to the Gd sublattice in $LiGd_{0.9}Ce_{0.1}P_4O_{12}$. Note that this 145 nm band is absent in the excitation spectrum of Ce^{3+} emission and apparently the transfer from phosphate group to Gd^{3+} is much more efficient than to Ce^{3+}. In the region of band-to-band transitions below 125 nm where free electrons and holes in the conduction and valence bands are created, the excitation efficiency of Gd^{3+} is much lower than that of Ce^{3+} ions. Apparently free electron–hole pairs have a high probability to recombine at Ce^{3+} ions.

4.2. High temperature studies ($T = 300$ K)

The excitation and emission spectra of cerium luminescence in $LiGd_{0.9}Ce_{0.1}P_4O_{12}$ ($\lambda_{em} = 327$ nm) in the fast time window at high temperatures ($T = 300$ K) as well as at low temperatures ($T = 10$ K) reveal bands typical for Ce^{3+} or recombinational processes involving Ce^{3+} (figure 5(a), curves 1 and 2). The excitation spectrum of Ce^{3+} luminescence for $\lambda_{em} = 327$ nm (figure 5(a), curve 2) shows the five bands typical for 4f–5d transitions (180–300 nm range) of Ce^{3+}. The luminescence spectrum also shows the emission doublet typical for the luminescence of Ce^{3+} (figure 5(a), curve 1). The main difference with the low temperature data is the broadening

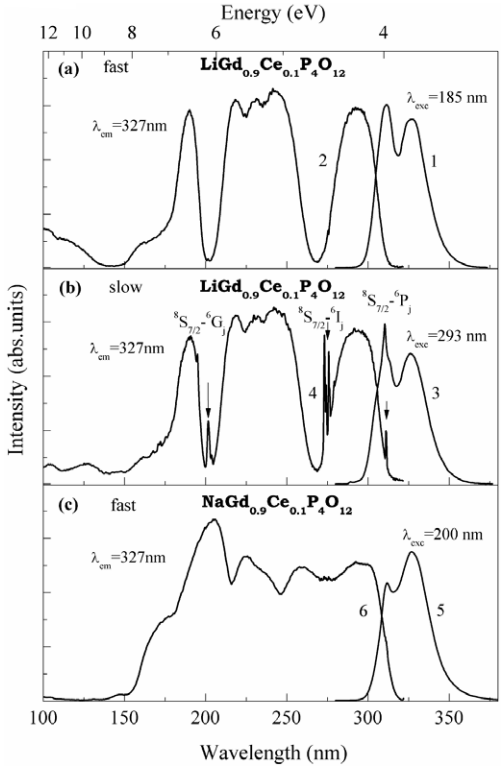

Figure 5. Excitation (2, 4, 6) and emission (1, 3, 5) spectra of $LiGd_{0.9}Ce_{0.1}P_4O_{12}$ and $NaGd_{0.9}Ce_{0.1}P_4O_{12}$ at 300 K. (a) Fast, (b) slow and (c) fast mode of registration.

of the excitation and emission bands at room temperature. It leads to part self-absorption of the short wavelength part of the cerium emission.

Another situation is realized in the case of luminescence registration in the slow time window, figure 5(b), curve 4. The excitation spectrum of Ce^{3+} luminescence now shows the f–f transitions of the Gd^{3+} ion in addition to the bands typical for cerium observed in the fast time window. In particular, the bands peaking at 205 nm related to $^8S_{7/2} \rightarrow {}^6G_j$ and at 273 nm $^8S_{7/2} \rightarrow {}^6I_j$ transitions are observed. The appearance of these bands shows energy transfer from Gd^{3+} to Ce^{3+} ions (Gd $\rightarrow$ Ce transfer). Such a transfer is possible due to the overlapping of Gd^{3+} emissions with the excitation band of Ce^{3+} luminescence. A contribution of Gd^{3+} ion emission with a maximum at $\lambda = 311$ nm also appears in the luminescence spectrum in the slow time window (figure 5(b), curve 3) upon excitation in Ce^{3+} absorption bands. Thus, the Gd $\rightarrow$ Ce energy transfer at 300 K is added in addition to the energy Ce $\rightarrow$ Gd transfer registered at 10 K.

Bidirectional energy transfer between Ce^{3+} and Gd^{3+} ions is shown in the decay curves of Ce^{3+} luminescence as well, see figure 6. Upon excitation in the cerium absorption band ($\lambda_{exc} =$ 290 nm), the decay kinetics at 300 K contains a fast component with decay constant of $\tau = 11.5$ ns and a slow component with $\tau \geqslant 10$ μs. The precise value of the slow component could not be measured because of equipment restrictions (figure 6, curve 1). The decay time constant of the fast component is slightly longer than the one of Ce^{3+} ($\tau = 9.5$ ns) at 10 K (figure 6, curve 2). Such lengthening of the decay constant

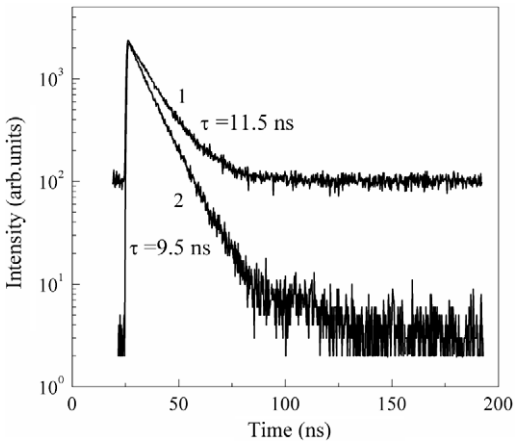

Figure 6. Luminescence decay curves of $LiGd_{0.9}Ce_{0.1}P_4O_{12}$ (curve 1 at 300 K and curve 2 at 10 K) under UV excitation ($\lambda_{exc} = 290$ nm, $\lambda_{em} = 330$ nm).

could be caused by the Gd $\rightarrow$ Ce back transfer as was observed in Lu-substituted Gd_2SiO_5–Ce crystals [17]. The presence of a slow component in the decay curve of the Ce^{3+} ion is typical for migration processes involving a Gd sublattice. Both the fast and slow components are also present in decay curves of Ce^{3+} ions under excitation in the Gd^{3+} absorption band at $\lambda_{em} = 273$ nm at $T = 300$ K.

4.3. Energy transfer

The temperature-dependent features in the excitation spectra and decay time kinetics of Ce^{3+} luminescence point to different mechanisms of energy transfer between Ce^{3+} and Gd^{3+} in $LiGd_{0.9}Ce_{0.1}P_4O_{12}$. In particular, the energy transfer from Ce^{3+} to Gd^{3+} is present at 10 K. This interaction is accompanied by the shortening of decay time kinetics of Ce^{3+} luminescence. The Ce $\rightarrow$ Gd energy transfer rate in such a system is about 5×10^8 s^{-1}. The scheme of energy levels and transitions of Ce^{3+} at $T = 10$ K are shown in figure 7(a). Because of the presence of an energy difference between the absorption edge of Ce^{3+} and the energy of the Gd^{3+} $^6P_{7/2} \rightarrow {}^8S_{7/2}$ transition the condition for Gd $\rightarrow$ Ce resonance energy transfer is not satisfied.

At a temperature of $T = 10$ K disregarding the resonance between the energy positions of the ^6D_j and ^6I_j levels of Gd^{3+} and the 5d levels of Ce^{3+}, the Gd $\rightarrow$ Ce energy transfer involving these energy levels does not occur. The energy transfer from Gd^{3+} to Ce^{3+} ions involving energy levels of ^6P_j (see figure 7(b)) is possible at $T = 300$ K due to temperature shift of the absorption edge of 5d–4f transitions of Ce^{3+} ions. Thus, the $^6P_{7/2}(Gd^{3+}) \rightarrow 5d(Ce^{3+})$ resonance interaction is a preferable mechanism of Gd $\rightarrow$ Ce energy transfer. The energy migration through the Gd sublattice to Ce^{3+} ion $(Gd–Gd–\cdots–Gd)_n$–Ce ensures the high conversion efficiency of high energy excitations in cerium emission.

5. X-ray-excited luminescence properties

In [2] the x-ray-excited luminescence properties of NaGd $(PO_3)_4$:10.0 at.% Ce^{3+} were reported, and it was established

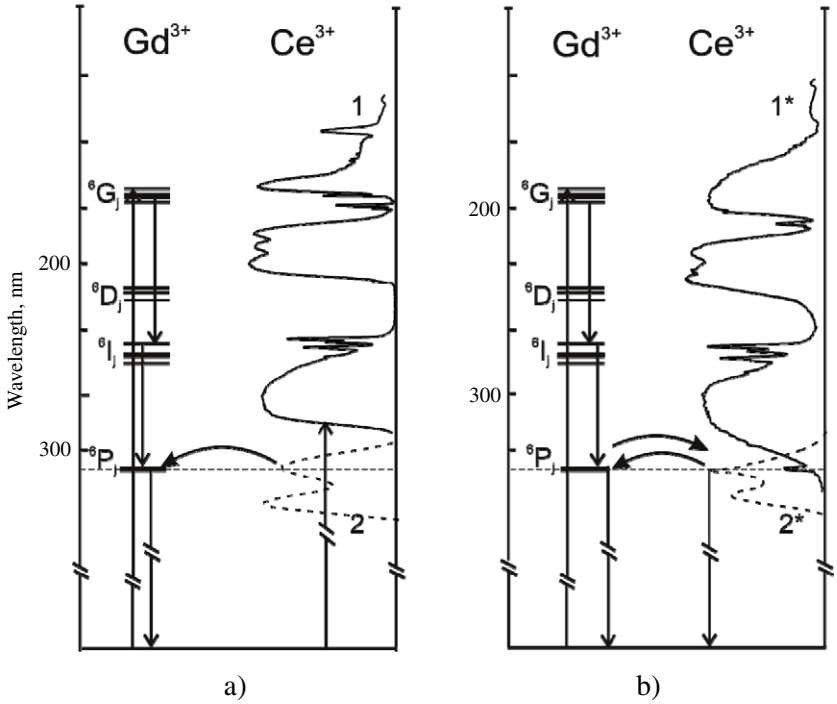

Figure 7. Energy transfer schemes of $LiGd_{0.9}Ce_{0.1}P_4O_{12}$ at 10 K (a) and 300 K (b). Excitation spectra of Gd^{3+} ion emission ((a), curve 1, $T = 10$ K) and excitation spectra of Ce^{3+} ion emission ((b), curve 1^*, $T = 300$ K). Emission spectra of $LiGd_{0.9}Ce_{0.1}P_4O_{12}$ ((a), curve 2, $T = 10$ K) and ((b), curve 2^*, $T = 300$ K).

that this phosphor possesses a high light yield. This is a positive characteristic for application as scintillator material for registration of x-rays or γ-rays. The luminescent parameters of $NaGdP_4O_{12}$:10.0 at.% Ce^{3+} were used to estimate the efficiency of $LiGd_{0.9}Ce_{0.1}P_4O_{12}$ and $LiY_{0.9}Ce_{0.1}P_4O_{12}$. The x-ray-excited emission spectra of the studied samples are shown in figure 8. X-ray-excited luminescence was measured in integral mode during a time window of 0–50 ns. The fast component of x-ray-excited emission of these samples shows double-peaked emission bands, which correspond to the two $5d–^2F_J$ transitions in Ce^{3+}.

In the x-ray-excited emission spectra of $NaGd_{0.9}Ce_{0.1}P_4O_{12}$ and $LiGd_{0.9}Ce_{0.1}P_4O_{12}$ the low intensity emission band of Gd^{3+} $^6P_{7/2} \rightarrow {}^8S_{7/2}$ at 311 nm is registered in integral mode, figures 8(a) and (b). The Gd-containing compounds $LiGd_{0.9}Ce_{0.1}P_4O_{12}$ and $NaGd_{0.9}Ce_{0.1}P_4O_{12}$ reveal slow components (figure 9(a)) with decay constants $\tau > 50$ μs in addition to a fast component with $\tau = 21.0$ and 18.0 ns, respectively. At the same time the $LiY_{0.9}Ce_{0.1}P_4O_{12}$ phosphor reveals only a fast component with $\tau = 24.7$ ns, figure 9(c). Since a slow component is not present for $LiY_{0.9}Ce_{0.1}P_4O_{12}$, this is an additional reason to suppose that the migration through the Gd sublattice leads to the appearance of the slow component in $LiGd_{0.9}Ce_{0.1}P_4O_{12}$ and $NaGd_{0.9}Ce_{0.1}P_4O_{12}$.

The intensities, decay time parameters and relative contributions of the fast decay time component of x-ray-excited luminescence are presented in table 2. A different efficiency of energy transfer from Gd^{3+} to Ce^{3+} can be caused by a different degree of overlap between the band peaked at 311 nm ($^6P_{7/2} \rightarrow {}^8S_{7/2}$ transition) with the Ce^{3+} absorption spectrum.

Table 2. Luminescence parameters of polyphosphate compounds.

Compounds	Intensity (arb. units)	Decay time of fast component (ns)	Contribution of fast component in luminescence spectrum (%)
$NaGd_{0.9}Ce_{0.1}P_4O_{12}$	1	18.0	10
$LiGd_{0.9}Ce_{0.1}P_4O_{12}$	0.6	21.0	10
$LiY_{0.9}Ce_{0.1}P_4O_{12}$	0.1	24.7	100

This overlap is better for $NaGd_{0.9}Ce_{0.1}P_4O_{12}$ (figure 5(c)) than for $LiGd_{0.9}Ce_{0.1}P_4O_{12}$ (figure 5(b)). Taking into account the tendency to increase the overlap between the Gd^{3+} luminescence spectrum and the Ce^{3+} absorption spectrum in $AGdP_4O_{12}$ (A = Li, Na, K, Cs) polyphosphates [3], one can expect that optimal conditions will be realized in the case of $CsGd(PO_3)_4$:10.0 at.% Ce^{3+}. Different parameters of the crystalline structure of $NaGd_{0.9}Ce_{0.1}P_4O_{12}$ (monoclinic space group $P2/n$) and $LiGd_{0.9}Ce_{0.1}P_4O_{12}$ (monoclinic space group $C2/c$) can also influence the transfer efficiency. One of the reasons for a higher emission intensity in $NaGd_{0.9}Ce_{0.1}P_4O_{12}$ relative to $LiGd_{0.9}Ce_{0.1}P_4O_{12}$ could be the larger size of the crystallites (200 μm relative to 5 μm). It may lead to a lower amount of defects in $NaGd_{0.9}Ce_{0.1}P_4O_{12}$ and a higher intensity of x-ray-excited luminescence.

6. Conclusions

An investigation of the luminescent parameters of $LiY_{0.9}Ce_{0.1}P_4O_{12}$, $LiGd_{0.9}Ce_{0.1}P_4O_{12}$ and $NaGd_{0.9}Ce_{0.1}P_4O_{12}$ powder

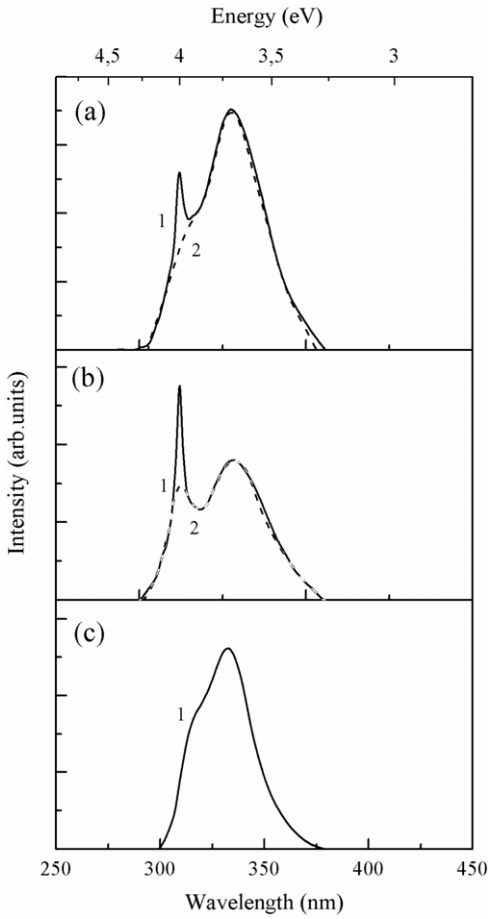

Figure 8. Normalized x-ray-excited emission spectra of $NaGd_{0.9}Ce_{0.1}P_4O_{12}$ (a), $LiGd_{0.9}Ce_{0.1}P_4O_{12}$ (b) and $LiY_{0.9}Ce_{0.1}P_4O_{12}$ (c) at 300 K; 1—integral and 2—fast mode.

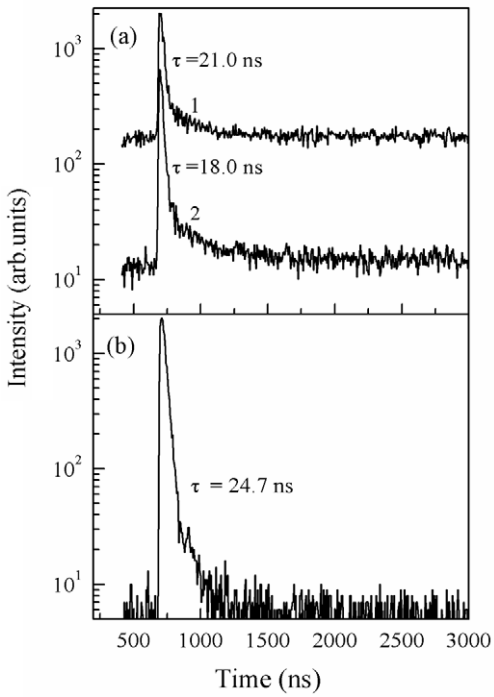

Figure 9. Decay time curves of x-ray-excited emission at 300 K: (a) $NaGd_{0.9}Ce_{0.1}P_4O_{12}$, (b) $LiGd_{0.9}Ce_{0.1}P_4O_{12}$ and (c) $LiY_{0.9}Ce_{0.1}P_4O_{12}$.

samples prepared by the melt solution technique was performed. In Gd-based samples, energy transfer processes between Ce^{3+} and Gd^{3+} have been revealed at low temperatures. Bidirectional energy transfer between Ce^{3+} and Gd^{3+} and energy migration through the Gd sublattice is observed at room temperature.

The presence of Gd^{3+} ions increases substantially the light yield of the investigated types of compounds. This is clearly seen from the comparison of light yields for $LiGd_{0.9}Ce_{0.1}P_4O_{12}$ and $LiY_{0.9}Ce_{0.1}P_4O_{12}$ which are isostructural and have the same concentration of Ce^{3+} ions. The higher value of light yield for $NaGd_{0.9}Ce_{0.1}P_4O_{12}$ is possibly caused by the better resonance between Gd^{3+} and Ce^{3+} levels, a possible smaller amount of defects in a grain and the difference in unit cell parameters of the crystal lattices. The contribution of the fast component (18.0 ns) in the scintillation pulse in Gd-containing phosphors is small. The predominant slow decay component is caused by migration processes through the Gd sublattice. This component is absent in $LiY_{0.9}Ce_{0.1}P_4O_{12}$ where the decay time constant is 24.7 ns.

Taking into account the efficiency of energy migration and transfer as a function of the lattice parameters, a further study of scintillation efficiency in polyphosphates with different cell unit parameters is of interest. Such systems for the study could be the $Gd_{1-x}Ce_xP_3O_9$ compounds which have distances between lanthanide ions of 4.7 Å against 5.6 Å in the investigated systems.

Acknowledgment

The work is partially supported by the Ukraine Ministry of Science and Education (grant no. 0109U002075).

References

[1] Zhong J, Liang H, Han B, Su Q and Tao Y 2008 *Chem. Phys. Lett.* **453** 192
[2] Zhong J, Liang H, Su Q, Dorenbos P and Danang Birowosuto M 2007 *Chem. Phys. Lett.* **445** 32
[3] Zhong J, Liang H, Lin H, Han B, Su Q and Zhang G 2007 *J. Mater. Chem.* **17** 4679
[4] Nikl M, Kamada K, Yoshikawa A, Krasnikov A, Beitlerova A, Solovieva N, Hybler J and Fucuda T 2006 *J. Phys.: Condens. Matter* **18** 3069
[5] Suzuki H, Tombrello T A, Mercher C L and Schweitzer J S 1994 *J. Lumin.* **60/61** 963
[6] Stoe WinX^{POW} 2007 *Version 2.21* Stoe & Cie GmbH, Darmstadt
[7] Rodriguez-Carvajal J 2001 *Comm. Powder Diffr. (IUCr) Newsl.* **26** 12
[8] Roisnel T and Rodriguez-Carvajal J 2000 *EPDIC7: Mater. Sci. Forum, Proc. Eur. Powder Diffr. Conf. (Barcelona)* p PB33
[9] Gelato L and Parthé E 1987 *Appl. J. Crystallogr.* **20** 139

[10] Zimmerer G 2007 *Radiat. Meas.* **42** 859
[11] Koizumi H 1976 *Acta Crystallogr.* B **32** 266
[12] Jouini A, Ferid M and Trabelsi-Ayadi M 2003 *Mater. Res. Bull.* **38** 437
[13] Ettis H, Naili H and Mhiri T 2006 *J. Solid State Chem.* **179** 3107
[14] Amami J, Ferid M and Trabelsi-Ayedi M 2005 *Mater. Res. Bull.* **40** 2144
[15] Dorenbos P, Pierron L, Dinca L, van Eijk C W E, Kahn-Harari A and Viana B 2003 *J. Phys.: Condens. Matter* **15** 511
[16] Voloshinovski A, Pidzyrailo N, Sol'skii I, Zimmerer G, Romanyshyn Yu and Struganyuk G 2004 *HASYLAB Ann. Report* vol 1, p 293
[17] Suzuki H, Tombrello T A, Melcher C L and Schweitzer J S 1994 *IEEE Trans. Nucl. Sci.* **41** 681